Synthesis, structural features, antibacterial behaviour and theoretical investigation of two new manganese(III) Schiff base complexes

Paul, Pranajit; Bhowmik, Kanti R. N.; Roy, Subhadip; Deb, Dibakar; Das, Nandita; Bhattacharjee, Maitri; Dutta Purkayastha, R. N.; Male, Louise; Mckee, Vickie; Pallepogu, Raghavaiah; Maiti, Debasis; Bauza, Antonio; Fontera, Antonio; Kirillov, Alexander M.

DOI:
10.1016/j.poly.2018.05.043

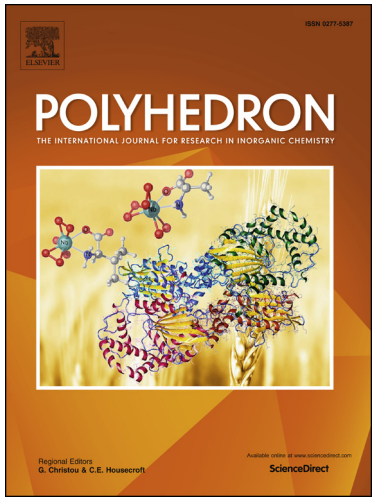

Synthesis, structural features, antibacterial behaviour and theoretical investigation of two new manganese(III) Schiff base complexes

Pranajit Paul, Kanti R.N. Bhowmik, Subhadip Roy, Dibakar Deb, Nandita Das, Maitri Bhattacharjee, R.N. Dutta Purkayastha, Louse Male, Vickie Mckee, Raghavaiah Pallepogu, Debasis Maiti, Antonio Bauza, Antonio Fontera, Alexander M. Kirillov

PII: S0277-5387(18)30281-X
DOI: https://doi.org/10.1016/j.poly.2018.05.043
Reference: POLY 13190

To appear in: *Polyhedron*

Received Date: 26 February 2018
Accepted Date: 18 May 2018

Please cite this article as: P. Paul, K.R.N. Bhowmik, S. Roy, D. Deb, N. Das, M. Bhattacharjee, R.N. Dutta Purkayastha, L. Male, V. Mckee, R. Pallepogu, D. Maiti, A. Bauza, A. Fontera, A.M. Kirillov, Synthesis, structural features, antibacterial behaviour and theoretical investigation of two new manganese(III) Schiff base complexes, *Polyhedron* (2018), doi: https://doi.org/10.1016/j.poly.2018.05.043

Synthesis, structural features, antibacterial behaviour and theoretical investigation of two new manganese(III) Schiff base complexes

Pranajit Paul[a], Kanti R. N. Bhowmik[a], Subhadip Roy[b], Dibakar Deb[a], Nandita Das[a], Maitri Bhattacharjee[a], R.N. Dutta Purkayastha[a,*], Louse Male[c], Vickie Mckee[d], Raghavaiah Pallepogu[e], Debasis Maiti[f], Antonio Bauza[g], Antonio Fontera[g,*], Alexander M. Kirillov[h]

[a]*Department of Chemistry, Tripura University, Suryamaninagar-799022, Tripura, India*

[b]*Department of Chemistry, IISER Bhopal, Bhopal Bypass Road, Bhauri, Bhopal-462066, M. P., India.*

[c]*School of Chemistry, University of Birmingham, Edgbaston, Birmingham B15 2TT, UK*

[d]*Department of Chemistry, Loughborough University, Loughborough, Leicestershire LE11 3TU, UK*

[e]*Department of Chemistry, Dr. Harisingh Gour University, Sagar-470003, Madhya Pradesh, India*

[f]*Department of Human Physiology, Tripura University, Suryamaninagar-799022, Tripura, India*

[g]*Departament de Quimica, Universitat de les Illes Balears, Crta. deValldemossa km 7.5, 07122 Palma de Mallorca (Baleares), Spain*

[h]*Centro de Química Estrutural, Instituto Superior Técnico, Universidade de Lisboa, Av. Rovisco Pais, 1049-001 Lisbon, Portugal*

* Corresponding authors. Addresses: Department of Chemistry, Tripura University, Suryamaninagar-799022, Tripura, India. Tel.:+919402137040 (R.N Dutta Purkayastha).
Departament de Quimica, Universitat de les Illes Balears, Crta. deValldemossa km 7.5, 07122 Palma de Mallorca (Baleares), Spain (A. Frontera).

E-mail addresses: rndp09@gmail.com (R.N. Dutta Purkayastha), *toni.frontera@uib.es* (A. Frontera).

Abstract

Two discrete manganese(III) coordination compounds, $[Mn(L)(OCN)]_2$ (**1**) and $[Mn(L')(H_2O)_2][dnba]\cdot DMF\cdot H_2O$ (**2**) bearing *in situ* generated Schiff base ligands H_2L [H_2L= *N*,*N*′-*o*-phenylenebis(salicylaldimine)] or H_2L' [H_2L'= *N*,*N*′-bis(salicylidene)ethylenediamine], were easily prepared by treating $Mn(CH_3COO)_2\cdot 4H_2O$ with salicylaldehyde and *o*-phenylenediamine (for **1**) or ethylenediamine (for **2**), and in the presence of supporting cyanate ligands or 3,5-dinitrobenzoate (dnba) counter anions, respectively. The obtained products were isolated as air-stable crystalline solids and were fully characterized by spectroscopic methods, single-crystal X-ray diffraction, topological analysis, as well as theoretical methods. The X-ray diffraction of the compound **1** reveals that the structure is dimeric with phenolic oxygen atom acting as bridge between two symmetrically equivalent Mn(III) atoms. The structure of **2** contains mononuclear cationic $[Mn(L')(H_2O)_2]$ units along with a 3,5-dinitrobenzoate anion and crystallization DMF molecule. Structural analysis indicates a distorted octahedral geometry for both complexes. Intermolecular hydrogen bonding and π-π stacking interactions are present in the lattice and play an important role in cohesion of the structures. Topological analysis of the compound **2** reveals a binodal 3,4-connected underlying 2D net with the 3,4L13 topology. Noncovalent interactions were investigated in terms of energies and geometries using theoretical calculations. Fluorescence and antibacterial properties of **1** and **2** were also investigated and discussed.

Keywords: Manganese; Schiff bases; Crystal structures; Noncovalent interactions; DFT calculations.

1. Introduction

The coordination chemistry of manganese has been an active area of research for decades [1]. One of the outstanding traits of manganese concerns a possibility of adopting a variety of oxidation states that is reflected in its diverse redox functions in several enzymes [2]. In addition to various *in vivo* and biomimetic roles, manganese compounds also exhibit interesting magnetic properties [3], intricate structures [4] and catalytic activity in a number of organic reactions [5].

Metal complexes of Schiff bases have been recognised as an important class of compounds with a wide range of applications as catalysts [6], metalloenzyme models [7], metallomesogens [8], nonlinear optical materials [9], building blocks for supramolecular structures [10], as well as antimicrobial [11], antiviral [12] or anticancer [13] agents. Although Schiff base complexes of manganese(III) are well known, they still continue to generate interest due to their important role in several metalloenzymes [14] and potential applications in the areas of catalysis [15] and magnetic materials [16].

Thus, to explore manganese(III) Schiff base chemistry and as a continuation of our interest in this research area, we report herein the synthesis, full characterization, spectroscopic, fluorescence, structural and topological features, antibacterial properties, as well as theoretical analysis of two novel manganese(III) complexes bearing *in-situ* generated Schiff base ligands, namely $[Mn(L)(OCN)]_2$ (**1**) and $[Mn(L')(H_2O)_2][dnba]\cdot DMF\cdot H_2O$ (**2**), wherein H_2L= *N*,*N*′-*o*-phenylenebis(salicylaldimine), H_2L'= *N*,*N*′-bis(salicylidene)ethylenediamine, dnba= 3,5-dinitrobenzoate, DMF= dimethylformamide.

2. Experimental

2.1. Materials and methods

Chemicals were of reagent grade and used without further purification. Solvents were purified by distillation prior to use. The FT-IR spectra were recorded as KBr discs using a Perkin Elmer 100 FT-IR spectrometer. Electronic spectra were recorded on a Perkin-Elmer model 1800 spectrophotometer. Magnetic susceptibility was measured by Gouy method using $Hg[Co(SCN)_4]$ as standard. Fluorescence spectra were obtained using a Fluorescence spectrophotometer model Fluorolog-3 Horiba Scientific. Antibacterial activity was evaluated using a molten agar disc diffusion method [17] and a broth culture method. C, H and N contents in the obtained compounds were ascertained using a Perkin Elmer CHN analyzer

(2400 series II). Manganese content in the compounds was determined by complexometric titration with EDTA using Erio-T as an indicator [18].

2.2. Synthesis of complexes

*2.2.1 Synthesis of [Mn(L)(OCN)]$_2$(**1**)[H_2L= N,N'-o-phenylenebis(salicylaldimine)]*

A solution containing $Mn(CH_3COO)_2 \cdot 4H_2O$ (0.2 g, 1.0 mmol) and NaOCN (0.1 g, 2.0 mmol) in 30 cm^3 of methanol was prepared (solution A). Another solution was obtained by refluxing salicylaldehyde (0.1 g, 1.0 mmol) and *o*-phenylenediamine (0.05 g, 0.5 mmol) in methanol (30 cm^3) for ca. 30 min (solution B). The solutions A and B were then mixed together and stirred in open air for *ca.* 2 h, resulting in a formation of a dark brown precipitate. The solid was collected by filtration and dissolved completely by slow addition of acetonitrile (25 cm^3), then stirred for 2 min and filtered. The filtrate was left undisturbed at room temperature for slow evaporation in air. The diffraction quality crystals of brown color were deposited within one week, separated by filtration, washed with methanol to give compound **1**. Yield 74%. *Anal*. Calc. for $C_{42}H_{28}Mn_2N_6O_6$: C, 61.32; H, 3.43; N, 10.22; Mn, 13.36. Found: C, 61.21; H, 3.40; N, 10.17; Mn, 13.25%. FTIR (KBr cm^{-1}) $1605_s\nu$ (C=N), $2175_s\nu_{as}(NCO^-)$, 1376 ν_s (NCO^-), 1313 ν(CO), 753 ν(Mn-O-Mn), 628 δ(NCO), 541 ν(Mn-N), 386 ν(Mn-O).

*2.2.2 Synthesis of [Mn(L')(H_2O)$_2$][dnba]·DMF·H_2O (**2**) (H_2L'= N,N'-bis(salicylidene)ethylenediamine, dnba= 3,5-dinitrobenzoate, DMF= dimethylformamide)*

$Mn(CH_3COO)_2 \cdot 4H_2O$ (0.2 g, 1.0 mmol) and 3,5-dinitrobenzoic acid (0.2 g, 1.0 mmol) were dissolved together in 15 cm^3 of aqueous methanol (1:1) to obtain a clear solution (solution A). Another solution (solution B) was prepared by dissolving together salicylaldehyde (0.1 g, 1.0 mmol) and ethylenediamine (0.03 g, 0.5 mmol) in 20 cm^3 of methanol, followed by heating the mixture under reflux for *ca.* 30 min. The solutions A and B were mixed together and the resulting mixture was stirred in open air for *ca*. 2 h, resulting in the precipitation of a brown microcrystalline product. This product was filtered off and then dissolved in 20 cm^3 of DMF-water mixture (1:1). The obtained filtrate was filtered again and then left undisturbed at room temperature for 4 days. Deep brown crystals suitable for X-ray diffraction studies were deposited, isolated by filtration, and washed with a small volume of methanol to give compound **2**. Yield 78%. *Anal.* Calc. for $C_{26}H_{30}MnN_5O_2$: Found: C, 47.34; H, 4.56; N, 10.62; Mn, 8.32, calcd: C, 47.35; H, 4.59; N, 10.62; Mn, 8.33. FTIR (KBr

cm^{-1}) 3108 ν(NH), 1621 ν(C=N), 1635 $\nu_{as}(COO^-)$, 1444 $\nu_s(COO^-)$, 1342 ν(CO), 756 $\rho_r(H_2O)$, 466 ν(Mn-N), 384 ν(Mn-O).

2.3. Crystallographic data collection and refinement

The intensity data for complexes **1** and **2** were collected at room temperature using a Bruker Smart Apex CCD diffractometer with graphite monochromated MoKα radiation (λ=0.71073Å). For data processing and absorption correction, the packages SAINT [19] and SADABS [20] were used. The crystal structures were solved by direct methods using SHELXS [21] and the refinement was carried out by full-matrix least-squares technique using SHELXL [21]. All non-hydrogen atoms were refined anisotropically. Hydrogen atom positions were calculated geometrically and refined using the riding model. In **1**, the cyanate group [N(3)–C(21)–O(3) / N(3′)–C(21′)–O(3′)] is disordered over two positions with the observed occupancy ratio of 0.697(16):0.303(16). Crystallographic data and structure refinement details for **1** and **2** are summarized in Table 1.

<Table 1>

2.4. Theoretical methods

All calculations were carried out using the TURBOMOLE version 5.9 [22] and the BP86-D3/def2-TZVP level of theory. To evaluate the interactions in the solid state, we applied the crystallographic coordinates. This procedure and level of theory were successfully used to evaluate similar interactions [23]. The interaction energies were computed by calculating the difference between the energies of isolated monomers and their assembly. The interaction energies were corrected for the Basis Set Superposition Error (BSSE) using the counterpoise method [24]. The "atoms-in-molecules" (AIM) [25] analysis was performed at the BP86-D3/def2-TZVP level of theory. The calculation of AIM properties was done using the AIMAll program [26].

2.5. Antibacterial activity

Antibacterial activity assay was tested against human pathogenic bacteria including *Klebsiella pneumonia, Shegella Flexneri 16, Shigella dysenteriae 1, Vibrio cholerae non-0139 (L4), V. cholerae non 0139 (CSK6669), Escherichia coli, Staphylococcus aureus and Streptococcus pneumonia.* The strains were treated with compounds **1**, **2** and ligands which were dissolved in DMSO. In determination of zone of inhibition, 5 mm Watmann filter paper

disc were placed on pre-spread bacteria in nutrient agar plate. After 14 hrs of incubation at 37 ^{o}C, the clear zone of inhibition was measured by scale. DMSO was used in the measurement as negative control. In broth culture, 50 µl of fresh overnight cultured bacterial cells were inoculated in 3 ml of broth media having different concentration of compounds **1**, **2** and ligands. After 14 hrs of shaking incubation, growth of bacteria was determined by optical density measurements at 600 nm. Only media with complex or ligands are considered as negative control (without bacteria).

3. Results and discussion

3.1. Synthesis and spectral characterization

The strategy adopted for synthesis of **1** and **2** was similar. In a typical reaction, the Schiff base ligands *N*,*N*′-*o*-phenylenebis(salicylaldimine) (H_2L) and *N*,*N*′-ethylenebis(saclicylaldimine) (H_2L') were generated *in situ* by a condensation reaction between *o*-phenylenediamine/ethylenediamine and salicylaldehyde in methanol solution, followed by a reaction with manganese(II) acetate and ancillary ligands, namely KOCN in case of **1** and 3,5-dinitrobenzoic acid for **2** in methanol solution. The manganese(II) ion undergoes an aerial oxidation to Mn(III) under the reaction conditions. A metal-assisted deprotonation of the phenolic moiety occurs during the formation of $[Mn(L)(OCN)]_2$ (**1**) and $[Mn(L')(H_2O)_2][dnba]\cdot DMF\cdot H_2O$ (**2**). Cyanate ion in **1** and water molecules in **2** present in the reaction solution get coordinated to the manganese(III) ion to complete a six-coordinate environment around the metal centres. The newly synthesized complexes were characterized by elemental analyses, spectral studies and by single crystal X-ray diffraction measurements. The compounds are air-stable and soluble in organic solvents viz. acetonitrile (**1**), DMF and DMSO (**1** and **2**).

The low molar conductivity (Λ_m) of 20-30 $\Omega^{-1}cm^2m^{-1}$ for compound **1** indicates that cyanate ion in the complex is coordinated to the metal centre and does not dissociate in the solution. In case of compound **2**, the molar conductivity of 78-81 $\Omega^{-1}cm^2m^{-1}$ is consistent with the values expected for 1:1 electrolyte [27]. FT-IR spectra of compounds **1** and **2** were analyzed and compared with those of the corresponding free ligands. Both the complexes show similar patterns, with a strong band observed between 1605-1621 cm^{-1} due to the imine ν(C=N) stretching vibration, which is red-shifted compared to the observed absorption for free ligands. A strong absorption band between 1332-1342 cm^{-1} due to phenolic C-O stretching also undergoes a shift to lower frequency with respect to free ligands, indicating a

deprotonation and subsequent coordination of the phenolic oxygen atoms to the metal centre. Compound **1** also reveals strong bands at *ca.* 2171 cm^{-1}, 1376 cm^{-1} and 628 cm^{-1} corresponding to $\nu_{as}(NCO^-)$, $\nu_s(NCO^-)$, and $\delta(NCO^-)$ modes of coordinated cyanato (NCO^-) ligand.

In case of compound **2**, additional bands were observed at 1635 cm^{-1} and 1342 cm^{-1} assignable to $\nu_{as}(COO^-)$ and $\nu_s(COO^-)$ modes of an uncoordinated 3,5-dinitrobenzoate anion. A band at *ca.* 3108 cm^{-1} probably arises from ν(NH) of the DMF moiety as evidenced by X-ray diffraction study (*vide supra*). Appearance of a strong band at 755 cm^{-1} for compound **1** is assignable to the 'Mn–O–Mn' vibration, resulting in a dimeric structure of the complex. The presence of a broad band in the IR spectrum of **2** at about 3400 cm^{-1} is associated with coordinated water molecule. Ligand coordination to the metal centre is further substantiated by prominent ν(Mn–N) bands between 466-511 cm^{-1}. All other characteristic vibrations due to the metal bound Schiff base are located in the range of 500-600 cm^{-1}.

3.2. Description of structures

*3.2.1. $[Mn(L)(NCO)]_2$ (**1**)*

Brown single crystals of the compound **1**, $[Mn(L)(NCO)]_2$, were obtained by slow evaporation from an acetonitrile solution and used for structural analysis. A schematic view of the structure is shown in Fig. 1 along with an atom labelling scheme. Compound **1** crystallizes in a monoclinic space group $P2_1/c$ and contains a binuclear manganese(III) entity, wherein the two centrosymmetrically related six-coordinate metal centres are interconnected by two weak phenoxo bridges. In each six-coordinated unit, the tetradentate (N_2O_2) Schiff base ligand occupies the equatorial position and the axial coordination takes place through *N*-atom of the pseudo-halide cyanate (NCO^-) moiety in a bent fashion. The characteristic bond distances and angles of the dimeric core in **1** are: Mn···Mn* 3.606(1) Å, Mn1–O1 (O1: intramolecular phenolate oxygen) 1.887(2) Å, Mn1–O1* (O1*: intermolecular phenolate oxygen) 2.828(2) Å, Mn1–O1*–Mn1* 97.78(7)° and O1–Mn1–O1* 82.22(7)° (*: 1-*x*,1-*y*,1-*z*). In an equatorial plane (O_2N_2), donor atoms are almost coplanar; however, the manganese atom deviates significantly from the equatorial plane by 0.245 Å. The coordination geometry of each of the Mn(III) ion is distorted octahedral with the elongation (Jahn-Teller distortion) along the OCN–Mn···O axis [16c,d]. This complex can be classified as a Type-1 out-of-plane dimer [28] and its bond lengths and angles are comparable to similar derivatives reported in literature [16d,28,29] (Table S1, Supporting information). Weak intermolecular hydrogen bonding interaction is present in the crystal lattice of **1** and provides further stabilization of

the structure. It is worth mentioning that both theoretical and experimental attempts have been directed earlier to correlate magnetic properties of out-of-plane dimeric Mn(III) Schiff base complexes with structural parameters [30]. It has been shown that structural parameters such as the Mn-O* distance and Mn-O*-Mn* angle have significant influences on magnetic coupling (*J*) with longer Mn-O* distances and lower Mn-O*-Mn* angle (~99˚) facilitating ferromagnetic interactions [30].

Furthermore, a search in the Cambridge Structural Database (CSD) [31] reveals that there are 68 structurally characterized manganese complexes derived from the Schiff base H_2L (substitution allowed). Among these, 22 examples feature di-manganese centres. Out of these, only 2 compounds [32] correspond to phenoxo bridged dimers similar to **1**. It indicates that formation of out-of-plane dimers is not favoured with H_2L. As a matter of fact, the Mn(III) complex with Schiff base H_2L and pseudohalide NCS^- is monomeric, [Mn(L)(NCS)] [33].

<Fig. 1>

*3.2.2. [Mn(L')(H_2O)$_2$][dnba]·DMF·H_2O (**2**)*

The crystal structure analysis reveals that the compound **2** crystallizes in the space group $P2_1/c$ and exists as mononuclear cationic species $[Mn^{III}(L')(H_2O)_2]^+$ [H_2L'=*N*,*N*′-ethylenebis(saclicylaldimine)] together with an uncoordinated 3,5-dinitrobenzoate anion and a crystallization molecule of DMF and H_2O. The structure of the complex (Fig. 2) exhibits a distorted octahedral geometry around the Mn(III) ion, which is coordinated by the tetradentate N_2O_2-donor Schiff base and two aqua ligands. The equatorial plane around the Mn(III) centre is occupied by two imine nitrogen [N1, N2] atoms and phenolic oxygen [O1, O2] atoms of Schiff base. The axial positions are taken by the oxygen atoms [O1W, O2W] of terminal water ligands. The Mn–O1W and Mn–O2W axial bonds of 2.224 (2) Å and 2.260 (2) Å are significantly longer than those of the Mn–O(1), Mn–O(2), Mn–N(1) and Mn–N(2) distances [1.877(2), 1.864(2), 1.978(3) and 1.971(3) Å, respectively]. These bond distances are typical for similar complexes [34]. The elongation of the axial bonds is indicative of Jahn–Teller distortion usually observed for high-spin Mn(III) complexes [34]. The deviation from the ideal octahedral geometry is also revealed by the values of equatorial and axial bond angles *viz.* 82.47(12)° to 93.40(9)°, and O1W–Mn1–O2W of 168.62(10)°, respectively.

<Fig. 2>

One of the aqua ligands is involved in H-bond formation with the DMF molecule [O1W···O31, 2.676(4) Å], while one of the carboxylate O atoms interacts with the 3,5-dinitrobenzoate anion [O1W···O22, 2.722 (3) Å]. The other H_2O ligand aqua is H-bonded to symmetry related (1+*x*,+*y*,+*z*) O22 atom of 3,5-dinitrobenzoate [O2W···O3W, 2.668(4) Å] and the symmetry related (1+*x*,3/2-*y*,1/2+*z*) O3W atom of the water ligand O2W···O22, 2.735(3) Å] from a neighbouring molecule. The water molecule of crystallization is also engaged in hydrogen bonding with the other carboxylate O-atom of the 3,5-dinitrobenzoate anion [O3W···O21, 2.730(4) Å], as well as with a symmetry related (+*x*,3/2-*y*,-1/2+*z*) O1 atom of DMF from another molecule. The details of the H-bonding distances are summarized in Table 2. The stability of the resulting H-bonded 2D layers is also reinforced by the π–π stacking interactions. Similar 2D network has been observed in $[Mn^{III}(H_2L_1)(CH_3OH)_2]Cl$ (H_4L_1= *N*,*N*′-bis(3-hydroxysalicylidene)ethane-1,2-diamine) [34a] where discrete units of cationic Mn^{III}-cores are self-assembled by chloride anion in the solid state through H-bonding.

A CSD search shows more than 305 structurally characterized manganese complexes derived from the Schiff base ligand H_2L' (substitution allowed). Nearly one-third of these contain mono-manganese centres. Among these, 26 examples represent mononuclear cationic species with uncoordinated anion similar to compound **2**. It has been found that the dimensionality of the supramolecular array in these compounds is governed by the nature of the anions which induce the self-assembly. Some notable anions include Cl^- [34a], PF_6^- [35a], NO_3^- [35a], ClO_4^- [35b], $[Fe(CN)_6]^{3-}$ [35c], 2,2′-bipyridine-4,4′-dicarboxylate [35d], Keggin-type $[SiW_{12}O_{40}]^{4-}$ [35e], and decavanadate [35f]. It is also important to mention here that the bulky nature of the 3,5-dinitrobenzoate could prevent the axial coordination to the manganese centre in comparison with related manganese Schiff base complexes bearing axially bound benzoate [36a], 3-chlorobenzoate [36b], 4-hydroxybenzoate [36c], or 3-nitrobenzoate [36d].

<Table 2>

3.3. Topological analysis of H-bonded network in compound ***2***

As mentioned above, the crystal packing of **2** reveals an extensive hydrogen bonding pattern between the $[Mn(L')(H_2O)_2]^+$ cations, 3,5-dinitrobenzoate(1–) anions and water molecules of crystallization (O3w), thus giving rise to the generation of a 2D H-bonded network (Fig. 3a). To get further insight into the structure of this network, we carried out its topological analysis by following the concept of the simplified underlying net [37]. Such a

net (Fig. 3b) was constructed by eliminating the terminal DMF moieties and contracting cations, anions, and solvent H_2O molecules to respective centroids, maintaining their connectivity via strong hydrogen bonds [D–H···A, wherein the H···A <2.50 Å, D···A <3.50 Å, and ∠(D–H···A) >120°; D and A stand for donor and acceptor atoms] [37a]. Topological analysis of this net reveals a binodal 3,4-connected underlying layer with the 3,4L13 topology. It is defined by the point symbol of $(4.6^2)_2(4^2.6^2.8^2)$ wherein the (4.6^2) and $(4^2.6^2.8^2)$ indices correspond to the 3-connected H_2O and 3,5-dinitrobenzoate(1–) nodes (topologically equivalent) and the 4-connected $[Mn(L')(H_2O)_2]^+$ nodes, respectively.

<Fig. 3>

3.4. Theoretical studies

The theoretical study is devoted to the analysis of the interesting noncovalent interactions observed in the solid state of the synthesized compounds **1** and **2**. As mentioned above, in the dimeric unit of **1**, the two centrosymmetrically related Mn(III) centres are held together by two phenoxo bridges. We were interested to compute the interaction energy of this dimer (dimerization energy). Hence, in compound **1**, we focused our attention on the interactions that lead to an infinite 1D ladder; these interactions are relevant to explain the crystal packing (Fig. 4A). Such an assembly is formed by the successive stacking of self-assembled Mn(III) dimers. The molecular electrostatic potential surface (MEP) for compound **1** has been computed and the most positive part of the surface is located close to the Mn(III) centre at the opposite side of the pseudohalide ligand. In addition, the negative potential at the coordinated phenolate O atom explains the formation of the self-assembled dimer. We have also evaluated the dimerization energy, which is large and negative (ΔE_1 = –36.9 kcal/mol), confirming the importance of the self-complementary Mn···O interactions. Furthermore, we also evaluated energetically the π-stacking complex (Fig. 4C) that is responsible for the formation of the infinite ladder. In addition to the π-stacking interaction, two unconventional C–H/π interactions are also established in which the π-system of the pseudohalide is involved. Electrostatically, this interaction is favoured since the potential value at the aromatic H-atom is positive (36 kcal/mol) due to an enhanced acidity of this hydrogen atom as a consequence of the coordination of the ligand to the Mn(III) centre. In addition, the electrostatic potential at the central C atom of the pseudohalide ligand is negative (–25 kcal/mol, Fig. 4B). The interaction energy of this complex (ΔE_2 = –30.4

kcal/mol) combines π–π and two C–H/π interactions (Fig. 4D). In an effort to evaluate the contribution of each interaction, we have computed an additional theoretical model where the pseudohalide ligands have been oriented oppositely (Fig. 4E). As a result, the interaction energy is reduced to ΔE_3 = –13.8 kcal/mol and corresponds to the π–π interaction. This interaction is larger than expected for this type of noncovalent bonding due to the presence of an extended π-system (two aromatic rings) and also owing to a large dipole–dipole term due to the metal coordination that increases the magnitude of the dipole and the antiparallel stacking mode. The contribution of each C–H/π interaction can be estimated as ½×(ΔE_2 – ΔE_3) = 8.3 kcal/mol.

<Fig. 4>

In compound **2**, we have studied the formation of infinite 1D H-bonded motifs in the solid state, which is governed by π–π stacking interactions and a hydrogen bonding network with participation of the uncoordinated water molecule (Fig. 5A). In particular, these water molecules interconnect the mononuclear Mn(III) units into 2D H-bonded layers (Fig. 3A). The dinitrobenzoate counter anion and DMF interact with the aromatic ligands by means of a combination of H-bonding and π–stacking interactions forming an interesting assembly. We have evaluated energetically both stacking interactions (Fig. 5, right). That is, using the Mn(III) complex interacting with the counter anion and the DMF molecules at one side of the aromatic ligand (Fig. 5B), we have computed the binding energies for the formation of the π–complexes at the opposite side, which are shown in Figs. 5C and 5D (3,5-dinitrobenzoate and DMF, respectively). The interaction with 3,5-dinitrobenzoate is very strong (ΔE_4 = –40.8 kcal/mol) due to the contribution of strong electrostatic effects between the anion and the cationic Mn(III) complex and also to the formation of a strong H-bonding interaction between the coordinated water molecule (enhanced acidic proton) and the anionic carboxylate group. We have also used a theoretical model (Fig. 5E) where this coordinated water molecule has been eliminated. If the same complex with 3,5-dinitrobenzoate is computed, the interaction is reduced ($\Delta E'_4$ = –26.5 kcal/mol) and corresponds to the stacking interaction, which can be also viewed as an anion–π interaction due to the anionic nature of the π-system. The difference $\Delta E_4 - \Delta E'_4$ = –14.3 kcal/mol corresponds to the strong $RCO_2^-\cdots H_2O$–Mn(III) H-bonding interaction. The π-interaction and H-bond with DMF present smaller interaction energy (Fig. 5D, ΔE_5 = –18.6 kcal/mol) due to the neutral nature of DMF. In case of using the theoretical model where the coordinated water molecule is eliminated,

the interaction energy is reduced to $\Delta E'_5 = -9.6$ kcal/mol that corresponds to the π–π stacking interaction between DMF and the complex, and the difference ($\Delta E_5 - \Delta E'_5 = -9.0$ kcal/mol) is the contribution of the H-bond.

<Fig. 5>

In compound **2**, we have also studied the existence of self-complementary antiparallel NO···NO interactions (blue dashed lines in Fig. 6A). These interactions in conjunction with bifurcated H-bonds are responsible for the formation of tetrameric units in the solid state. The importance of similar $NO_3 \cdots NO_3$ interactions between coordinated nitrato ligands has been highlighted in the solid state structure of hetero bimetallic Cu(II)–uranyl complexes with Schiff-base ligands [38] and nitrato co-ligands and more recently between nitrato co-ligands of *N*-benzimidazolyl-pyrimidine–Cu(II) complexes [39]. We have evaluated the interaction energy ($\Delta E_5 = -12.5$ kcal/mol) of this tetramer as a dimer; only the antiparallel NO···NO and bifurcated H-bonds were evaluated (red and blue dashed lines). In an effort to evaluate the contribution of the antiparallel NO···NO interaction, we have computed a theoretical model (Fig. 6B) where only the 3,5-dinitrobenzoate moieties were considered. As a result, the interaction energy is reduced to $\Delta E_6 = -4.7$ kcal/mol that is a rough estimate of the antiparallel NO···NO interaction.

Finally, we have used Bader's theory of "atoms-in-molecules", which provides an unambiguous definition of chemical bonding, to characterize the non covalent NO···NO interactions described above. In Fig. 6C we show the AIM analysis of the dimer and the NO···NO interaction is characterized by the presence of one bond critical point that connects the symmetrically related oxygen atoms of the nitro substituents, thus confirming the existence of the interaction. The value of the Laplacian of the charge density computed at the bond critical point is positive, being common in closed-shell interactions.

<Fig. 6>

3.5. Electronic spectra

Electronic spectra (10^{-4} M) of the H_2L and H_2L' ligands were measured in methanol solution. Ligand H_2L shows absorptions at *ca.* 316-328 nm (ε_m= 13920-15230 $mol^{-1}cm^{-1}L^{-1}$) and a medium intensity band at *ca.* 290 nm (ε_m= 8560 $mol^{-1}cm^{-1}L^{-1}$), whereas H_2L' shows an

absorption band at *ca.* 331nm (ε_m= 4940 $mol^{-1}cm^{-1}L^{-1}$). The observed absorption for H_2L' is assignable to intra-ligand charge transfer (ILCT) transition. However lower intensity absorption for H_2L' arises due to intra-ligand π-π* transition.

The UV visible spectra (10^{-4} M) for the complexes **1** and **2** were recorded in acetonitrile and dimethylformamide solutions, respectively (Fig. S1, Supporting information). Absorptions for compound **1** were observed in the range of 317-330 nm (ε_m= 1087 $mol^{-1}cm^{-1}L^{-1}$). For compound **2**, an absorption band was observed at *ca.* 405 nm (ε_m= 3540 $mol^{-1}cm^{-1}L^{-1}$). The observed transition for the complexes can be assigned to phenolate (pπ)→Mn(III) (dπ) charge transfer by analogy with similar Mn(III) complexes [15c].

3.6. Room temperature magnetic study

Complexes **1** and **2** show room temperature magnetic moments of 4.84 BM (per Mn centre) and 4.76 BM, respectively, which are close to the spin only value for high spin d^4 manganese(III) ion. Although a detailed investigation of magnetic properties of **1** and **2** including variable temperature magnetic measurements is out of the scope of the present investigation, compound **1** may show interesting magnetic features. Previous reports indicate that Mn^{III} Schiff base out-of-plane dimers are promising candidates for single-molecule magnets as the phenoxide pathway can mediate ferromagnetic exchange couplings, leading to a spin ground state of $S_T = 4$ [40].

3.7. Fluorescence studies

Photoluminescence behaviour of the ligands (H_2L and H_2L') and compounds (**1** and **2**) was investigated in DMSO solution. Steady state fluorescence studies were employed as independent evidence of complexation between the ligands and metal ions. The ligand H_2L displays prominent emission at 459 nm on excitation at 328 nm, while ligand H_2L' exhibits emission at 434 nm on excitation at 330 nm. It is important to mention here that compound **2** is nonfluorescent, while compound **1** shows a broad emission at 421 nm on excitation at 330 nm (Fig. S2, Supporting information). The observed emissions for the ligands are assignable to π(L)→π*(L) transitions and possess an intraligand charge transfer (ILCT) character. The broad nature of emission band of **1** indicates a charge transfer nature of the transition.

The emission for **1** is blue-shifted in comparison to free ligand and assignable to intra-ligand π-π* transition [41]. The fluorescence quantum yield of compound **1** is found to be higher than that of the ligand H_2L (Table S2, Supporting information). Appreciable difference

in position of emission maximum and higher fluorescence quantum yield in **1** support a complexation process. The quenching of fluorescence of ligand by transition metal ion during the complexation is a common phenomenon, which is explained by processes such as magnetic perturbation, redox-activity andelectronic energy transfer [42a,b]. The nonfluorescent nature of compound **2** might be due to any of the processes mentioned above.

3.8. Antibacterial activity

The obtained antibacterial activity data are shown in Table 3 in terms of zone of inhibition and minimum inhibitory concentration (MIC). The activity of free ligands and Mn(III) complexes was screened against eight human pathogenic bacteria including *Klebsiella pneumonia*, *Shegella Flexneri 16*, *Shigelladysentriae 1*, *Vibrio cholerae non. 0139*, *Escherichia coli, Staphylococcus aureus* and *Streptrococcus pneumonia* using disk diffusion method and broth culture method. The results of antibacterial screening indicate that H_2L and H_2L' are not active. However, complex **1** exhibits an appreciable antibacterial activity. The inhibition zone data show that **1** is active against *Shigella dysentriae 1, Vibrio cholera non. 0139, Escherichia coli,* and *Staphylococcus aureus*; the MIC values are 400µg/ml in all cases. Compound **2** is less active showing MIC values of 500 µg/ml for *Vibrio cholera non. 0139, Escherichia coli,* and *Streptrococcus pneumonia*; for other human pathogenic strains investigated herein, the inhibition of bacterial growth is not very significant.

<Table 3**>**

4. Conclusions

In the present work, we have synthesized two new manganese(III) complexes (**1** and **2**) that bear two different N_2O_2-Schiff base ligands generated *in situ*. The obtained compounds have been fully characterized, by spectroscopic methods, single-crystal X-ray diffraction, topological analysis and DFT calculations. Two centrosymmetrically related manganese(III) centres are held together by the phenoxy bridges resulting in a dimeric structure in the complex **1**, while the compound **2** represents a mononuclear cationic complex. The solid state structures of both products show participation of the Schiff base ligand and anionic co-ligands in concurrent hydrogen bonding, π-hole and π-stacking interactions that control crystal packing patterns. The difference in Schiff base ligands and

co-ligands employed during the synthesis as well as diverse noncovalent interactions present in the compounds have led to the structural diversity between **1** and **2**.

In compound **1**, the ancillary Mn(III)···O and π-stacking interactions have been energetically studied and confirmed their importance in the solid state. In compound **2**, the nitro substituents of the 3,5-dinitrobenzoate are involved in antiparallel NO···NO interaction that has been confirmed by AIM analysis of critical points and bond paths. This experimental investigation also supports the importance of π-stacking and NO···NO interactions in solid state chemistry. In addition, the computational study has highlighted the impact of these unconventional interactions on the final structure. Such analyses of supramolecular arrangements in manganese Schiff base complexes are significantly less explored in literature [43]. The computation of the energetic features of the different noncovalent interactions is important to gain knowledge about the processes that govern supramolecular chemistry and crystal packing.

Besides, the results of antibacterial screening indicate that the compound **1** shows an appreciable antibacterial activity against different types of pathogenic bacteria. Further research aiming at the synthesis of related types of manganese(III) compounds and search for their functional applications (e.g., magnetic behavior) will be pursued.

Acknowledgements

Authors R.N.D.P, K.R.N.B, P.P, D.D, N.D and M.B are thankful to the authority of Tripura University, Suryamaninagar for providing infrastructure facility. S.R acknowledges SERB, Government of India (File number PDF/2017/001188) for National Post-doctoral fellowship. A.B and A.F thank DGICYT of Spain (project CONSOLIDER INGENIO CSD2010-00065, FEDER funds) for funding. We also thank the CTI (UIB) for free allocation of computer time. A.M.K. acknowledges the Foundation for Science and Technology (FCT) and Portugal 2020 (LISBOA-01-0145-FEDER-029697, UID/QUI/00100/2013). We also thank the reviewers for their helpful comments at the revision stage.

Appendix A. Supplementary material

CCDC 857299 and 938779 contain the supplementary crystallographic data for **1** and **2**, respectively. These data can be obtained free of charge via http://www.ccdc.cam.ac.uk/conts/retrieving.html, or from the Cambridge Crystallographic

Data Centre, 12 Union Road, Cambridge CB2 1EZ, UK; fax: (+44) 1223-336-033; or e-mail: deposit@ccdc.cam.ac.uk.

References

[1] (a) K.C. Mondal, Y. Song, P.S. Mukherjee, Inorg. Chem. 46 (2007) 9736–9742;

(b) K.C. Mondal, M.G.B. Drew, P.S. Mukherjee, Inorg. Chem. 46 (2007) 5625–5629;

(c) P. Kar, R. Haldar, C.J. Gomez-Garcia, A. Ghosh, Inorg. Chem. 51 (2012) 4265−4273;

(d) X. Ma, D. Zhao, L.-F. Lin, S.-J. Qin, W.-X. Zheng, Y.-J. Qi, X.-X. Li, S.-T. Zheng, Inorg. Chem. 55 (2016) 11311−11315;

(e) K. Chattopadhyay, G.A. Craig, M.J. Heras Ojea, M. Pait, A. Kundu, J. Lee, M. Murrie, A. Frontera, D. Ray, Inorg. Chem. 56 (2017) 2639–2652.

[2] (a) G. Christou, Acc. Chem. Res. 22 (1989) 328–335;

(b) K. Wieghardt, Angew. Chem. Int. Ed. Engl. 28 (1989) 11533–1172;

(c) L. Que, A.E. True, Prog. Inorg. Chem. 38 (1990) 97–200;

(d) S. Mukhopadhayay, S.K. Mandal, S. Bhaduri, W.H. Armstrong, Chem. Rev. 104 (2004) 3981–4026.

[3] (a) L.K. Thompson, O. Waldmann, Z. Xua, Coord. Chem. Rev. 249 (2005) 2677–2690;

(b) S. Naiya, S. Biswas, M.G.B. Drew, C.J Gomez-Garcia, A. Ghosh, Inorg. Chem. 51 (2012) 5332–5341;

(c) A. Konstantatos, R. Bewley, A.-L. Barra, J. Bendix, S. Piligkos, H. Weihe, Inorg. Chem. 55 (2016) 10377–10382;

(d) M.P. Bubnov, I.A. Teplova, E.A. Kopylova, K.A. Kozhanov, A.S. Bogomyakov, M.V. Petrova, V.A. Morozov, V.I. Ovcharenko, V.K. Cherkasov, Inorg. Chem. 56 (2017) 2426–2431.

[4] (a) M. Soler, W. Wernsdorfer, K. Folting, M. Pink, G. Christou, J. Am. Chem. Soc. 126 (2004) 2156–2165;

(b) T.C. Stamatatos, G. Christou, Inorg. Chem. 48 (2009) 3308–3322;

(c) U. García-Couceiro, O. Castillo, J. Cepeda, M. Lanchas, A. Luque, S. Pérez-Yáñez, P. Román, D. Vallejo-Sánchez, Inorg. Chem. 49 (2010) 11346–11361.

(d) G.-N. Liu, G.-C. Guo, F. Chen, S.-H. Wang, J. Sun,J.-S. Huang, Inorg. Chem. 51 (2012) 472–482.

[5] (a) M.M. Najafpour, M. Amini, M. Holynska, M. Zare, E. Amini, New J. Chem. 38 (2014) 5069-5074;

(b) T.K. Mukhopadhyay, C.L. Rock, M. Hong, D.C. Ashley, T.L. Groy, M.-H. Baik, R.J. Trovitch, J. Am. Chem. Soc. 139 (2017) 4901-4915.

[6] P.G. Cozzi, Chem. Soc. Rev. 33 (2004) 410–421.

[7] (a) M. Ohashi, T. Koshiyama, T. Ueno, M. Yanase, H. Fujii, Y. Watanabe, Angew. Chem. Int. Ed. 42 (2003) 1005-1008;

(b) N. Yokoi, T. Ueno, M. Unno, T. Matsui, M. Ikeda-Saito, Y. Watanabe, Chem. Commun. (2008) 229–231.

[8] M. Marcos, J.L. Serrano, T. Sierra, M.J. Gimenez, Chem. Mater. 5 (1993) 1332–1337.

[9] J.P. Costes, J.F. Lamère, C. Lepetit, P.G. Lacroix, F. Dahan, K. Nakatani, Inorg. Chem. 44 (2005) 1973–1982.

[10] N. Yoshida, K. Ichikawa, M. Shiro, J. Chem. Soc., Perkin Trans. 2 (2000) 17–26.

[11] M.S. Nair, D. Arish, R.S. Joseyphus, J. Saud. Chem. Soc. 16 (2012) 83–88.

[12] K.S. Kumar, S. Ganguly, R. Veerasamy, E. De Clercq, Eur. J. Med. Chem. 45 (2010) 5474–5479.

[13] N. Zhang, Y.-h. Fan, Z. Zhang, J. Zuo, P.-f. Zhang, Q. Wang, S.-b. Liu, C.-f. Bi, Inorg. Chem. Commun. 22 (2012) 68–72.

[14] E.J. Larson, V.L. Pecoraro, in: V.L. Pecoraro (Ed.), Manganese Redox Enzymes, VCH Publisher, Inc., New York, 1992, p. 1.

[15] (a) E.N. Jacobsen, in: I. Ojima (Ed.), Catalytic Asymmetric Synthesis, VCH, Weinheim, 1993, p. 159;

(b) T. Katsuki, in: I. Ojima (Ed.), Catalytic Asymmetric Synthesis, 2nd ed., Wiley, New York, 2000, p. 287;

(c) S. Majumder, S. Hazra, S. Dutta, P. Biswas, S. Mohanta, Polyhedron 28 (2009) 2473–2479.

[16] (a) H. Miyasaka, R. Clérac, W. Wernsdorfer, L. Lecren, C. Bonhomme, K.-I. Sugiura, M. Yamashita, Angew. Chem. 116 (2004) 2861–2865;

(b) H. Miyasaka, T. Nezu, K. Sugimoto, K.I. Sugiura, M. Yamashita, R. Clérac, Chem. Eur. J. 11 (2005) 1592–1602.

(c) G. Bhargavi, M.V. Rajasekharan, J.P. Costes, J.P. Tuchagues, Polyhedron 28 (2009) 1253-1260;

(d) G. Bhargavi, M.V. Rajasekharan, J.P. Tuchagues, Inorg. Chim. Acta 362 (2009) 3247-3252;

(e) J. Nishijo, T. Yoshida, M. Enomoto, Polyhedron 87 (2015) 233–236.

[17] (a) A. Barry, in: V. Lorian (Ed.), Antibiotics in Laboratory Medicine, Williams and Wilkins, Baltimore, MD, 1991, pp. 1–16; (b) T. Rosu, M. Negoiu, S. Pasculescu, Eur. J. Med. Chem. 45 (2010) 774–781.

[18] A.I. Vogel, A Textbook of Quantitative Inorganic Analysis, 3rd ed., Longman Green and Co Ltd, New York, 1964.

[19] SAINT, Data Reduction and Frame Integration Program for the CCD Area-Detector System. Bruker Analytical X-ray Systems, Madison, Wisconsin, USA, 1997–2006.

[20] G.M. Sheldrick, SADABS, Program for Area Detector Adsorption Correction, Institute for Inorganic Chemistry, University of Göttingen, Germany, 1996.

[21] G.M. Sheldrick, Acta Crystallogr. Sect. C 71 (2015) 3–8.

[22] R. Ahlrichs, M. Bär, M. Hacer, H. Horn, C. Kömel, Chem. Phys. Lett. 162 (1989) 165–169.

[23] (a) D. Sadhukhan, M. Maiti, G. Pilet, A. Bauzá, A. Frontera, S. Mitra, Eur. J. Inorg. Chem. 11 (2015) 1958–1972;

(b) M. Mirzaei, H. Eshtiagh-Hosseini, Z. Bolouri, Z. Rahmati, A. Esmaeilzadeh, A. Hassanpoor, A. Bauza, P. Ballester, M. Barceló-Oliver, J.T. Mague, B. Notash, A. Frontera, Cryst. Growth Des. 15 (2015) 1351–1361;

(c) P. Chakraborty, S. Purkait, S. Mondal, A. Bauzá, A. Frontera, C. Massera, D. Das, CrystEngComm 17 (2015) 4680–4690;

(d) A. Bauzá, A. Terrón, M. Barceló-Oliver, A. García-Raso, A. Frontera, Inorg. Chim. Acta. 452 (2016) 244–250.

[24] S.F. Boys, F. Bernardi, Mol. Phys. 19 (1970) 553–566.

[25] R.F.W. Bader, Chem. Rev. 91 (1991) 893–928.

[26] AIMAll (Version 13.05.06), T. A. Keith, TK Gristmill Software, Overland Park KS, USA, 2013.

[27] W.J. Geary, Coord. Chem. Rev. 7 (1971) 81–122.

[28] H. Miyasaka, R. Clerac, T. Ishii, H.C. Chang, S. Kitagawa, M. Yamashita, J. Chem. Soc., Dalton Trans., (2002) 1528-1534.

[29] (a) L. Lecren, W. Wernsdorfer, Y.G. Li, A. Vindigni, H. Miyasaka, R. Clérac, J. Am. Chem. Soc. 129 (2007) 5045–5051;

(b) R. Karmakar, C.R. Choudhury, G. Bravic, J.P. Sutter, S. Mitra, Polyhedron 23 (2004) 949–954;

(c) H.L. Shyu, H.H. Wei, Y. Wang, Inorg. Chim. Acta 290 (1999) 8–13;

(d) Y. Feng, C. Wang, Y. Zhao, J. Li, D. Liao, S. Yan, Q. Wang, 362 (2009) 3563–3568;

(e) S. Saha, D. Mal, S. Koner, A. Bhattacherjee, P. Gutlich, S. Mondal, M. Mukherjee, K.I. Okamoto, Polyhedron 23 (2004) 1811–1817;

(f) H.H. Ko, J.H. Lim, H.C. Kim, C.S. Hong, Inorg. Chem. 45 (2006) 8847–8849;

(g) Z.L. Lu, M. Yuan, F. Pan, S. Gao, D.Q. Zhang, D.B. Zhu, Inorg. Chem. 45 (2006) 3538–3548.

[30] P. Seth, S. Giri, A. Ghosh, Dalton Trans., 44 (2015) 12863-12870.

[31] F.H. Allen, Acta Crystallogr., Sect. B 58 (2002) 380-388.

[32] (a) E. Gallo, E. Solari, N. Re, C. Floriani, A. Chiesi-Villa, C. Rizzoli, J. Am. Chem. Soc., 119 (1997) 5144-5154;

(b) K. Ha, Acta Crystallogr., Sect. E 66 (2010) m233-m234.

[33] S. Biswas, K. Mitra, C.H. Schwalbe, C. Robert Lucas, S.K. Chattopadhyay, B. Adhikary, Inorg. Chim. Acta, 358 (2005) 2473-2481.

[34] (a) M.R. Bermejo, F. M. Isabel, G.N. Ana M., M. Marcelino, P. Rosa, R. M. Jesús, V. Miguel, Eur. J. Inorg. Chem., (2004) 2769-2774;

(b) M.R. Bermejo, F.M. Isabel, G.F. Esther, G.N. Ana, M. Marcelino, P. Rosa, R.M. Jesús, Eur. J. Inorg. Chem., (2007) 3789-3797;

(c) M. Ángeles Vázquez-Fernández, M. Isabel Fernández-García, A.M. González-Noya, M. Maneiro, M.R. Bermejo, M. Jesús Rodríguez-Doutón, Polyhedron, 31 (2012) 379-385.

[35] (a) A. Gutiérrez, M.F. Perpiñán, A.E. Sánchez, M.C. Torralba, V. González, Inorg. Chim. Acta, 453 (2016) 169-178;

(b) R. Li, J. Tian, H. Liu, S. Yan, S. Guo, J. Zhang, Transition Met. Chem., 36 (2011) 811-817;

(c) H. Miyasaka, H. Okawa, A. Miyazaki, T. Enoki, J. Chem. Soc., Dalton Trans., (1998) 3991-3996;

(d) T.-T. Cao, Y. Ma, C. Yang, D.-Z. Liao, S.-P. Yan, J. Coord. Chem., 63 (2010) 3093-3100;

(e) X. Meng, H.-N. Wang, X.-L. Wang, G.-S. Yang, S. Wang, K.-Z. Shao, Z.-M. Su, Inorg. Chim. Acta, 390 (2012) 135-142;

(f) S. Lin, Q. Wu, H. Tan, E. Wang, J. Coord. Chem., 64 (2011) 3661-3669.

[36] (a) V.S. Thampidas, T. Radhakrishnan, R.D. Pike, Acta Crystallogr. Sect. E, 64 (2008) m150-m151;

(b) T. Kikunaga, T. Matsumoto, T. Ohta, H. Nakai, Y. Naruta, K.-H. Ahn, Y. Watanabe, S. Ogo, Chem. Commun., 49 (2013) 8356-8358.

(c) R. Reshma, P.V. Soumya, S.M. Simi, V.S. Thampidas, R.D. Pike, Acta Crystallogr. Sect. E, 65 (2009) m1110-m1111.

(d) V.S. Thampidas, T. Radhakrishnan, R.D. Pike, Acta Crystallogr. Sect. E, 64 (2008) m990-m991.

[37] (a) V. A. Blatov, IUCr CompComm Newsletter, 7 (2006) 4–38;

(b) V. A. Blatov, A. P. Shevchenko, D. M. Proserpio, Cryst. Growth Des. 14 (2014) 3576–3586.

[38] S. Ghosh, S. Biswas, A. Bauzá, M. Barceló-Oliver, A. Frontera, A. Ghosh, Inorg. Chem., 52 (2013) 7508–7523.

[39] S. Canellas, A. Bauza, A. Lancho, A. Garcia-Raso, J.J. Fiol, E. Molins, P. Ballester, A. Frontera, CrystEngComm, 17 (2015) 5987-5997.

[40] (a) H. Miyasaka, A. Saitoh, S. Abe, Coord. Chem. Rev., 251 (2007) 2622-2664;

(b) W. Ting-Ting, R. Min, B. Song-Song, Z. Li-Min, Eur. J. Inorg. Chem., 2014 (2014) 1042-1050.

[41]. D. Dey, S. Roy, R.N. Dutta Purkayastha, R. Pallepogu, L. Male, V. McKee, J. Coord. Chem. 64 (2011) 1165-1176.

[42] (a) N. Chattopadhyay, A. Mallick, S. Sengupta, J. Photochem. Photobiol. A 177 (2005) 55;

(b) P. Purkayastha, G.K. Patra, D. Datta, N. Chattopadhyay, Indian J. Chem. A 39 (2000) 375.

[43] (a) N. Sarkar, K. Harms, A. Frontera, S. Chattopadhyay, New J. Chem., 41 (2017) 8053-8065;

(b) N. Sarkar, M.G.B. Drew, K. Harms, A. Bauza, A. Frontera, S. Chattopadhyay, CrystEngComm, 20 (2018) 1077-1086;

(c) S. Banerjee, P. Brandao, A. Bauza, A. Frontera, M. Barcelo-Oliver, A. Panja, A. Saha, New J. Chem., 41 (2017) 11607-11618.

Table 1. Crystallographic data and structure refinement for **1** and **2**.

Empirical formula	$C_{42}H_{28}Mn_2N_6O_6$ (**1**)	$C_{26}H_{30}MnN_5O_{12}$ (**2**)
Formula weight	822.58	659.49
Temperature/K	293(2)	298(2)
Crystal system	Monoclinic	Monoclinic
Space group	$P2_1/c$	$P2_1/c$
a/Å	10.0161(5)	7.2860(10)
b/Å	14.4552(7)	29.489(4)
c/Å	13.1972(6)	13.6274(18)
α/°	90.00	90.00
β/°	106.7480(10)	90.039(2)
γ/°	90.00	90.00
Volume/Å^3	1829.70(15)	2928.0(7)
Z	2	4
ρ_{calc}g/cm^3	1.493	1.496
μ/mm^{-1}	0.749	0.523
F(000)	840.0	1368.0
Crystal size/mm^3	0.20 × 0.20 × 0.10	0.42 × 0.30 × 0.08
Radiation	MoKα (λ = 0.71073)	MoKα (λ = 0.71073)
2θ range for data collection/°	6.44 to 50.06	2.76 to 52.08
Index ranges	$-11 \le h \le 11$, $-17 \le k \le 17$, $-15 \le l \le 15$	$-8 \le h \le 8$, $-36 \le k \le 36$, $-16 \le l \le 16$
Reflections collected	21539	30135
Independent reflections	3217 [R_{int} = 0.0571]	5735 [R_{int} = 0.0616]
Data/restraints/parameters	3217/60/281	5735/9/417
Goodness-of-fit on F^2	1.015	1.108
Final R indexes [$I \ge 2\sigma(I)$]	R_1 = 0.0384, wR_2 = 0.0815	R_1 = 0.0631, wR_2 = 0.1375
Final R indexes [all data]	R_1 = 0.0615, wR_2 = 0.0916	R_1 = 0.0864, wR_2 = 0.1476
Largest diff. peak/hole / e Å^{-3}	0.26/-0.28	0.47/-0.28

Table 2. Hydrogen bonding parameters in compound **2**.

D	H	A	d(D-H)/Å	d(H-A)/Å	d(D-A)/Å	D-H-A/°
O1W	H1WA	O22	0.811(18)	1.914(18)	2.722(3)	173(4)
O1W	H1WB	O31	0.808(18)	1.868(18)	2.676(4)	179(5)
O2W	H2WA	O22[1]	0.819(18)	1.92(2)	2.735(3)	170(4)
O2W	H2WB	O3W[2]	0.827(18)	1.87(2)	2.668(4)	161(4)
O3W	H3WA	O1[3]	0.816(19)	2.14(2)	2.941(4)	170(6)
O3W	H3WB	O21	0.828(19)	1.90(2)	2.730(4)	176(6)

[1] 1+x,+y,+z; [2] 1+x,3/2-y,1/2+z; [3] +x,3/2-y,-1/2+z

Table 3. Antibacterial activity of compounds **1** and **2**.

(a) Effect of complex **1**

Bacterial strain		Concentration of complex **1** (µg/disc or µg/ml)				MIC (µg/ml)
Klebsiella pneumonia		400	100	10	0	
	Zone of Inhibition (mm)	10.3 ± 0.57	8.6 ± 0.89	6.2 ± 0.44		
	O.D. at 600 nm	No growth	0.66 ± 0.21	1.13 ± 0.17	1.09± 0.2	400
Shegella Flexneri 16	Zone of Inhibition (mm)	8.6 ± 1.15	8 ± 1.6	6.75 ± 0.95		
	O.D. at 600 nm	No growth	0.46 ± 0.3	1.08 ± 0.13	1.11± 0.24	-
Shigella dysenteriae 1	Zone of Inhibition (mm)	9.0 ± 1.0	8.2 ± 0.44	6.0 ± 0.0		
	O.D. at 600 nm	No growth	0.54 ± 0.07	1.08 ± 0.13	0.74± 0.33	-
Vibrio cholerae non-0139 (L4)	Zone of Inhibition (mm)	9.3 ± 1.52	9.0 ± 2.44	6.75 ± 0.95		
	O.D. at 600 nm	No growth	0.49 ± 0.04	0.93 ± 0.43	1.0± 0.39	400
V. cholerae non 0139 (CSK6669)	Zone of Inhibition (mm)	8.0 ± 1.52	7.5 ± 0.7	6.5 ± 0.7		
	O.D. at 600 nm	No growth	0.35 ± 0.11	0.92 ± 0.14	1.18± 0.36	-
Escherichia coli	Zone of Inhibition (mm)	8.3 ± 2.3	7.6 ± 1.3	6.0 ± 0.0		
	O.D. at 600 nm	0.25 ± 0.17	0.65 ± 0.12	0.97 ± 0.11	0.97± 0.1	400
Staphylococcus aureus	Zone of Inhibition (mm)					
	O.D. at 600 nm	No growth	0.41 ± 0.31	0.94 ± 0.09	1.1± 0.15	400
Streptococcus pneumoniae	Zone of Inhibition (mm)	10.0 ± 0	8.5 ± 0.7	6.6 ± 1.15		
	O.D. at 600 nm	No growth	0.61 ± 0.39	1.05 ± 0.18	1.13± 0.15	400

(b) Effect of complex **2**

Bacterial strain		Concentration of complex **2** (µg/disc or µg/ml)				MIC (µg/ml)
Klebsiella pneumonia		400	100	10	0	
	Zone of Inhibition (mm)	10.0 ± 0.0	8.25 ± 0.5	6.25 ± 0.5		
	O.D. at 600 nm	0.24 ± 0.09	0.48 ± 0.16	0.78 ± 0.18	0.74± 0.23	-
Shegella Flexneri 16	Zone of Inhibition (mm)	10.3 ± 3.21	9 ± 1.4	7.0 ± 1.15		
	O.D. at 600 nm	0.43 ± 0.08	0.49 ± 0.11	0.85 ± 0.32	0.75± 0.27	-
Shigella dysenteriae 1	Zone of Inhibition (mm)	9.6± 0.57	8.6 ± 0.54	6.0 ± 0.0		
	O.D. at 600 nm	No growth	0.62 ± 0.21	0.79 ± 0.19	0.88± 0.31	-
Vibrio cholerae non-0139 (L4)	Zone of Inhibition (mm)	11.0 ± 0.0	10.5 ± 0.58	6.75 ± 0.95		
	O.D. at 600 nm	No growth	0.53 ± 0.15	0.78 ± 0.17	0.78± 0.28	500
V. cholerae non 0139 (CSK6669)	Zone of Inhibition (mm)		8.0± 0.0	6.0 ± 0.0		
	O.D. at 600 nm	0.14 ± 0.18	0.77 ± 0.2	0.96 ± 0.17	0.98± 0.15	-
Escherichia coli	Zone of Inhibition (mm)	9.0 ± 1.4	7.5 ± 1.3	6.3 ± 0.57		
	O.D. at 600 nm	No growth	0.65 ± 0.19	0.83 ± 0.22	0.96± 0.27	500
Staphylococcus aureus	Zone of Inhibition (mm)					
	O.D. at 600 nm	No growth	0.67 ± 0.18	0.88 ± 0.09	0.79± 0.15	-
Streptococcus pneumoniae	Zone of Inhibition (mm)	10.0 ± 0	9.0 ± 1.0	6.0 ± 0.0		
	O.D. at 600 nm	0.25 ± 0.23	0.61 ± 0.12	1.11 ± 0.19	1.07± 0.11	500

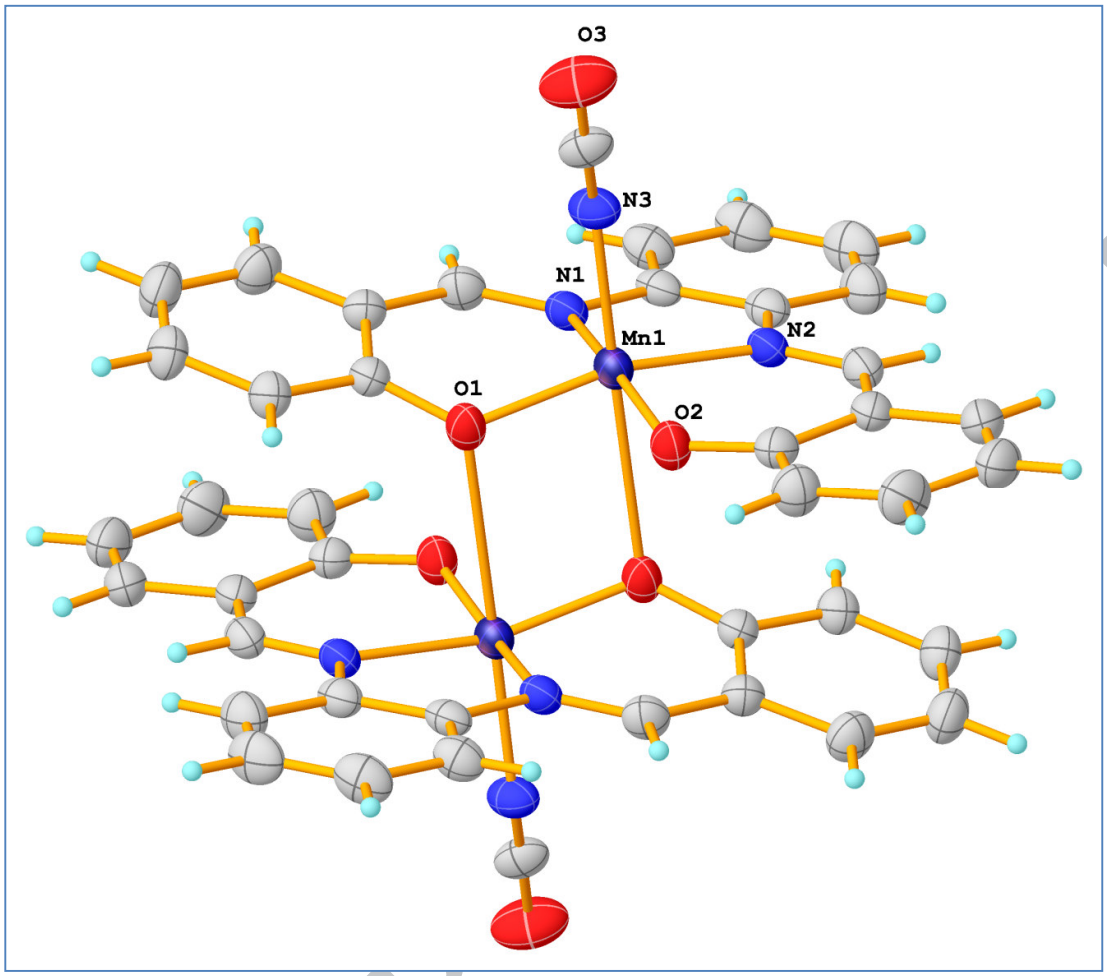

Fig.1. Crystal structure of $[Mn(L)(NCO)]_2$ (**1**). Colour codes: Mn (violet balls), C (grey), O (red), N (blue), H (pale blue). Only the major component of the disordered cyanate ligand is shown.

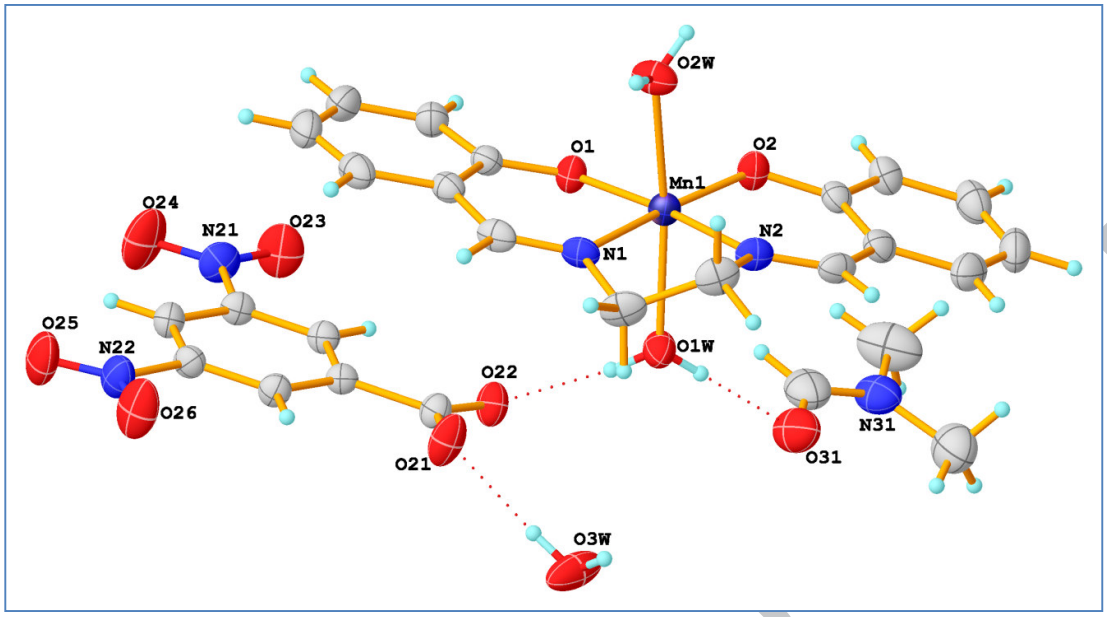

Fig. 2. Crystal structure of $[Mn(L')(H_2O)_2][dnba]\cdot DMF\cdot H_2O$ (**2**). Colour codes: Mn (violet balls), C (grey), O (red), N (blue), H (pale blue). H bonds are shown as thin dotted lines.

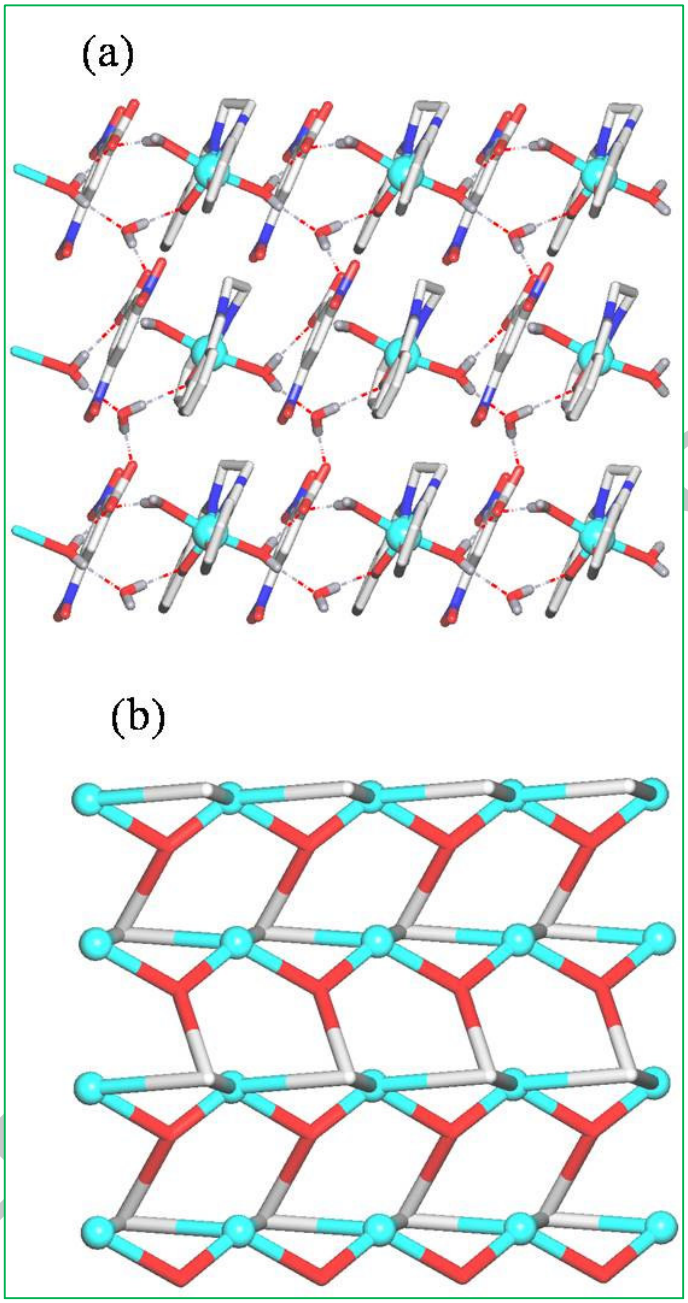

Fig. 3. Structural fragments of **2**: (a) 2D H-bonded network and (b) its topological representation showing a binodal 3,4-connected underlying net with the 3,4L13 topology (views along the *b* axis). Further details: (a) H atoms (apart from those participating in H-bonds) and DMF moieties were omitted for clarity, colour codes: Mn (cyan balls), C (grey), O (red), N (blue), H (dark gray); (b) centroids of 4-connected $[Mn(L')(H_2O)_2]^+$ cations (cyan balls), centroids of 3-connected 3,5-dinitrobenzoate(1–) anions (grey), centroids of 3-coonected H_2O molecules of crystallization (red).

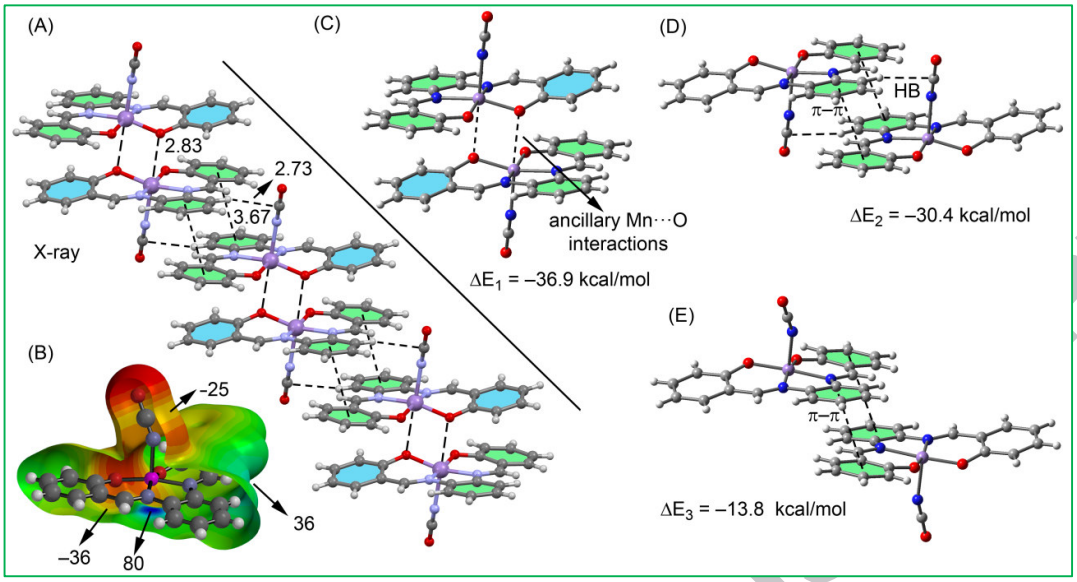

Fig. 4. (A) Structural fragment of compound **1**. (B) MEP surface of complex **1**. (C–D) Theoretical models used to evaluate the noncovalent interactions.

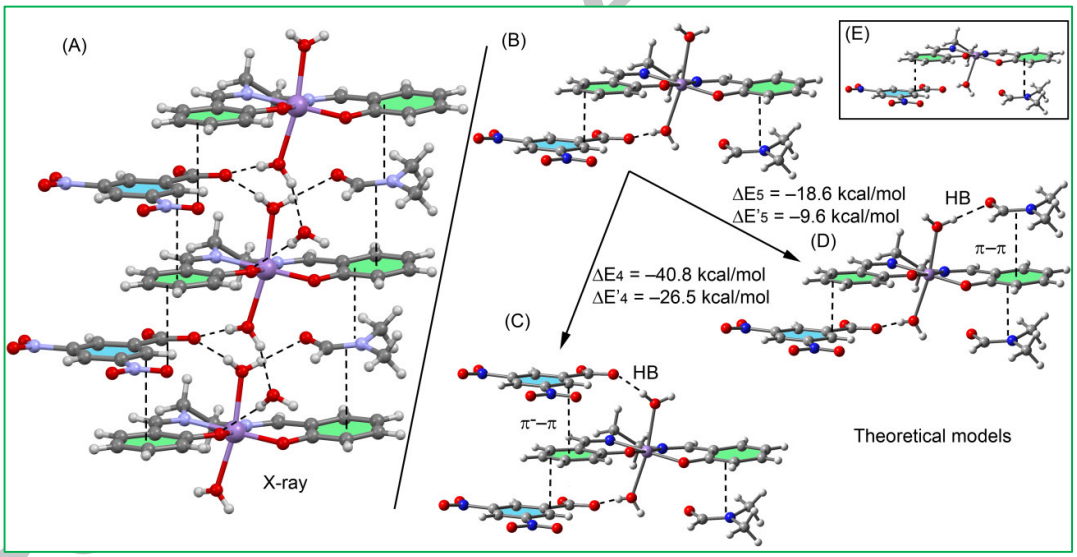

Fig. 5. (A) Structural fragment of compound **2**. (B–E) Theoretical models used to evaluate the noncovalent interactions.

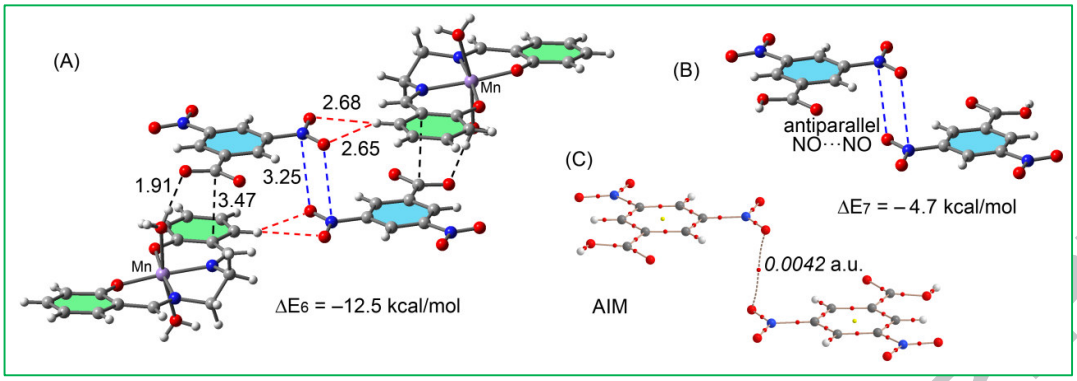

Fig. 6. (A) Structural fragment of compound **2**. (B) Theoretical models used to evaluate the NO···NO interaction. (C) AIM analysis of compound **2**. Bond and ring critical points are represented by red and yellow spheres, respectively. The bond paths connecting bond critical points are also represented.

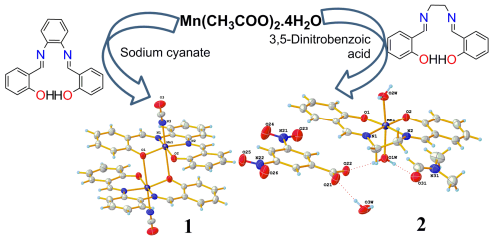

Synopsis

Manganese(III) Schiff base compounds, $[Mn(L)(OCN)]_2$ (**1**), $[Mn(L')(H_2O)_2][dnba]\cdot DMF\cdot H_2O$ (**2**) [H_2L= *N*,*N*′-*o*-phenylenebis(salicylaldimine)] or H_2L' [H_2L'= *N*,*N*′-bis(salicylidene)ethylenediamine], were prepared and characterized by spectroscopic and X-ray diffraction analysis. Theoretical study analyses noncovalent interactions in the complexes. Topological analysis of **2** reveals existence of binodal 3,4-connected 2D net with the 3,4L13 topology. Fluorescence and antibacterial properties of the compounds were also explored.

Graphical Abstract